was performed using a differential scanning calorimeter (DSC) (Q-10, TA Instruments, New Castle, DE, U.S.A.) and software (Universal Analysis 2000, TA Instruments). Aliquots of aqueous solutions (10 μl) in aluminum cells were cooled from room temperature at 10 °C/min, and then scanned from −70 °C at 5 °C/min. The effect of heat-treatment (annealing) on the thermal properties of the frozen solutions was studied after the initial heating scan paused at −10 °C, then the samples were maintained at this temperature for 10 min. Thermal data were acquired in the subsequent heating from −70 °C at 5 °C/min. Freeze-dried solids (1—2 mg) in hermetic aluminum cells were subjected to the thermal analysis from −20 °C at 5 °C/min under nitrogen gas flow. Melted organic acids (approx. 5 mg, 200 °C) in aluminum cells were rapidly cooled to −50 °C, and then scanned at 5 °C/min to obtain the glass transition temperatures. Glass transition temperatures were determined as the midpoint (maximum inflection) of the discontinuities in the heat flow curves.

Powder-X-Ray Diffraction (XRD) The powder X-ray diffraction patterns were measured at various temperatures by using a Rint-Altima diffractometer (Rigaku, Tokyo, Japan) with Cu$K\alpha$ radiation at 40 kV/40 mA. The samples were scanned in the area of $5°<2\theta<35°$ at an angle speed of 15°/min by heating at 2 °C/min from room temperature.

Mid- and Near-Infrared Analysis A Fourier-transform infrared spectrophotometer (MB-104, Bomen, Quebec, Canada) with a gas generator (Balston, Haverhill, MA, U.S.A.) and Grams/32 software were used to obtain mid-infrared spectra of freeze-fried solids. Approximately 0.5 mg of the solid was mixed with dried KBr powder (250 mg) and made into tablets by compression. The KBr tablets were scanned 128 times to obtain the spectra in the 400—4000 cm^{-1} region. Near-infrared spectroscopy was performed by using a Bruker MPA system with a diffuse-reflectance integrating-sphere probe (PbS detector) and OPUS software (Ettlingen, Germany). Near-infrared light was directed upward from the bottom of the glass vials containing freeze-dried solids to obtain the reflected signal over a range of 4000—12000 cm^{-1} with a resolution of 4 cm^{-1} in 128 scans. The freeze-dried solids were measured twice by rotating the sample vials between measurements.

Activity of Lactate Dehydrogenase in Freeze-Dried Solids Aqueous solutions (250 μl) containing LDH (0.05 mg/ml) and excipients were freeze-dried in flat-bottom glass vials (10 mm diameter). One of the enzyme solutions was freeze-dried at a higher sodium phosphate buffer concentration (50 mM, pH 7.0). Other enzyme solutions contained the added excipients and lower concentration buffer components (<1 mM) diluted from the dialyzed protein solutions. Activity of LDH was obtained spectrophotometrically at 25 °C. Each 1.0 ml of assay mixture contained 0.35 mM pyruvic acid and 0.07 mM reduced nicotinamide-adenine dinucleotide (NADH) in 50 mM sodium phosphate buffer (pH 7.5). The enzyme reaction was started by the addition of LDH solution (50 μl), and the decrease in the absorbance at 340 nm was monitored. The enzyme activity (%) relative to that before freezing was shown.

Results

Physical Property of Frozen Solutions The thermal profiles of frozen solutions containing L-histidine and citric acid at various concentration ratios (total 200 mM) are shown in Fig. 1. The single-solute frozen L-histidine solution (200 mM) showed a T_g' (glass transition temperature of maximally freeze-concentrated solute) at −33.5 °C, and an exotherm peak that suggests eutectic crystallization at around −8 °C.[12] Freeze-drying of solutions at above their T_g' often induces physical collapse because of the significantly reduced local viscosity in the freeze-concentrated phase.[1] The second scan of the 200 mM L-histidine solutions after the heat-treatment (−10 °C, 10 min) gave flat thermograms that indicate crystallized solute up to the ice melting temperature (data not shown). The citric acid solution (200 mM) had a T_g' at −55.1 °C, indicating that the solute remained amorphous in the freeze-concentrated phase surrounding ice crystals. The L-histidine crystallization peak disappeared in the presence of citric acid. The two-solute frozen solutions showed transitions (T_g's) at temperatures as high as −22.8 °C at the equal (100 mM) L-histidine and citric acid concentrations.

Figure 2 shows transition temperatures (T_g') of frozen solutions containing amino acids and organic acids at various concentration ratios. Some single-solute frozen amino acid or organic acid solutions (200 mM) had apparent T_g' transitions at −44.2 °C (L-arginine), −55.1 °C (citric acid), and

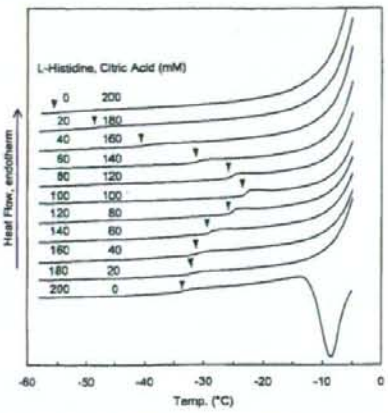

Fig. 1. Thermal Profiles of Frozen Solutions Containing L-Histidine and Citric Acid

Aliquots (10 μl) of solutions in hermetic aluminum cells were scanned from −70 °C at 5 °C/min. Glass transition temperatures of maximally freeze-concentrated solutes (T_g') are indicated by inverted triangles (▼).

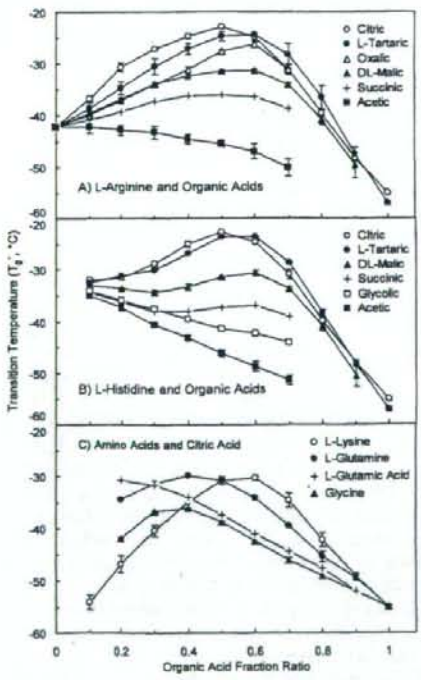

Fig. 2. Glass Transition Temperatures of Maximally Freeze-Concentrated Solute (T_g') in Frozen Solutions Containing an Amino Acid and an Organic Acid at Varied Concentration Ratios (Total 200 mM, Average±S.D., $n=3$)

−57.1 °C (L-tartaric acid). The frozen L-glutamine solution showed both T'_g (−42.8 °C) and the subsequent eutectic crystallization peak (approx. −25 °C) in the heating scan (data not shown). Thermograms of the frozen L-lysine and DL-malic acid solutions inclined gradually without apparent transition up to the ice melting endotherm, which suggested T'_gs lower than −60 °C. Exotherm peaks either in the cooling process (glycine, acetic acid) or in the heating scan (oxalic acid) indicated eutectic crystallization in the frozen solution.[16] Potential T'_g transitions of some frozen solutions that also showed eutectic crystallization peaks (*e.g.*, 200 mM L-histidine or L-glutamine) were not included in the figure. The limited solubility of some amino acids and organic acids (*e.g.*, L-glutamic acid, fumaric acid, maleic acid) prevented them from undergoing thermal analysis at 200 mM. A lower concentration glutamic acid solution (100 mM) showed a T'_g at −32.2 °C and an exotherm peak that suggests eutectic crystallization at around −11.0 °C (data not shown).

Mixing of the solutes induced some unique physical properties in the frozen solutions that depend on the number of functional groups in the consisting molecules. The transition temperatures (T'_gs) of frozen solutions containing a basic or neutral amino acid (L-histidine, L-arginine, L-lysine, L-glutamine, glycine) and a hydroxy di- or tricarboxylic acid (citric acid, L-tartaric acid, DL-malic acid) showed bell-shaped profiles. The frozen solutions containing a hydroxy di- or tricarboxylic acid (citric acid, L-tartaric acid) and an acidic amino acid (L-glutamic acid) did not show the mixing-induced upward T'_g shift. Citric acid also effectively prevented the crystallization of glycine in the frozen solutions. Dicarboxylic acids (succinic acid, maleic acid, fumaric acid, oxalic acid) showed a high tendency to crystallize in the single-solute frozen solutions and in some mixture frozen solutions.[15,17] The frozen solutions containing L-arginine and oxalic acid or succinic acid also presented the high transition temperature (T'_g) by mixing. A mono-carboxylic acid (acetic acid), a hydroxy mono-carboxylic acid (glycolic acid), and HCl did not show the upward T'_g shift in the mixture with the basic amino acids.[13]

Physical Property of Freeze-Dried Solids Freeze-drying of the single-solute amino acid solutions resulted in cylindrical cakes that showed varied crystallinity in the powder X-ray diffraction (XRD) and thermal analyses (Figs. 3, 4). Freeze-dried L-arginine showed the typical harrow XRD pattern of amorphous solids. Thermal scan of the solid showed the glass transition (52.6 °C) and subsequent crystallization exotherm (105—110 °C). Freeze-dried L-histidine showed largely amorphous XRD pattern (30 °C) with the broad glass transition (65—100 °C) and crystallization at varied temperatures (120—150 °C). The L-arginine and L-histidine solids showed apparent crystallization peaks in the XRD patterns at the elevated temperature (150 °C). The dried L-glutamine (200 mM) solids showed features of both crystalline (*e.g.*, peaks in the XRD pattern) and amorphous (*e.g.*, glass transitions and heat-induced crystallization exotherm) solids. The solute concentration in the initial solution and thermal history in the freeze-drying process should determine the crystallinity of the freeze-dried L-histidine and L-glutamine.[12] Glycine was freeze-dried as β polymorph crystal.[18] Freeze-drying of citric acid or L-tartaric acid solutions (200 mM) resulted in unstructured or particulate solids that

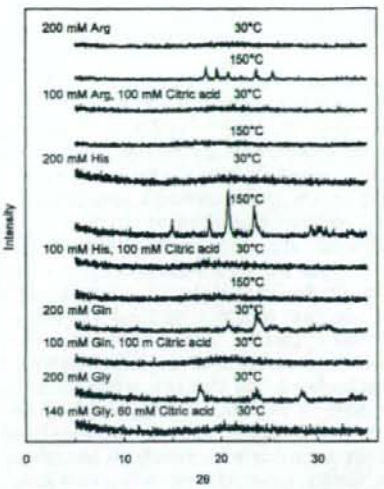

Fig. 3. Powder X-Ray Diffraction Patterns of Freeze-Dried Solids Containing Amino Acids and Citric Acid

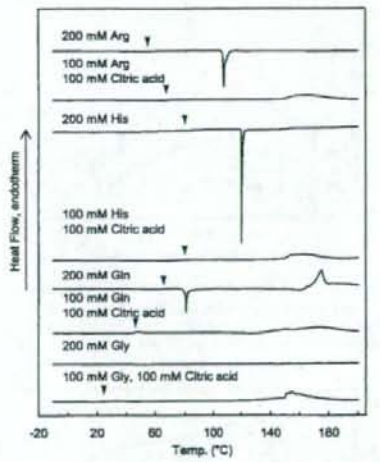

Fig. 4. DSC Thermograms of Freeze-Dried Solids Containing Amino Acids and Citric Acid

Freeze-dried solids (1—2 mg) in hermetic aluminum cells were scanned from −20 °C at 5 °C/min.

indicate physical collapse in the primary during process. Amorphous solids of the organic acids prepared by rapid-cooling of the melt liquid showed glass transition at 9.2 °C (citric acid) and 68.1 °C (L-tartaric acid) in the thermal scan ($n=3$).[19]

Co-lyophilizing the basic or neutral amino acids (L-arginine, L-histidine, L-glutamine, glycine) and the organic acid (citric acid, L-tartaric acid) produced cylindrical non-crystalline cake solids at wide initial concentration ratios (Figs. 3—5). The solids obtained by freeze-drying the basic amino acids (L-arginine, L-histidine) with citric or L-tartaric acid showed glass transition at temperatures (T_gs) much higher

than those of the individual components. The transitions were observed at temperatures as high as 89.5 °C (140 mM L-arginine, 60 mM citric acid) or 98.5 °C (160 mM L-histidine, 40 mM citric acid). Shrinking of some solids containing higher ratio of organic acid during the freeze-drying process suggested their low glass transition temperatures. The XRD and thermal analysis also indicated that the co-lyophilized solids remained amorphous up to 150 °C. Some binary freeze-dried solids showed a broad endotherm that suggests component decomposition at the elevated temperatures. The mixing of L-arginine with citric acid and with L-tartaric acid showed similar T_g profiles, in spite of the large difference in their transition temperatures of the cooled-melt solids. The bell-shaped profiles of the transition temperatures were significantly different from the reported transitions of binary nonionic molecule systems that follow Gordon–Taylor equation.[20] Glass transition temperatures of amorphous solids containing ideally mixed nonionic molecules without particular attractive or repulsive interactions shift between those of the individual components. Contrarily, the glass transition temperatures of co-lyophilized L-glutamine and citric acid combination solids shifted linearly between those of the individual components, which suggested absence of the particular attractive interactions between the heterogeneous molecules in the solids. Co-lyophilization of glycine and citric acid resulted in amorphous cake solids only at limited molar ratios.

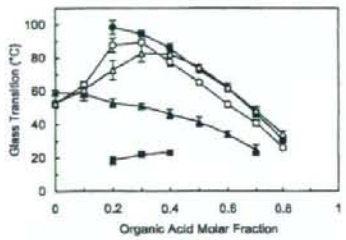

Fig. 5. Glass Transition Temperatures of Freeze-Dried Binary Solids

Each symbol denotes transition of solids containing L-arginine and citric acid (○), L-arginine and tartaric acid (△), L-histidine and citric acid (●), L-glutamine and citric acid (▲), or glycine and citric acid (■) (total: 200 mM, average±S.D., $n=3$).

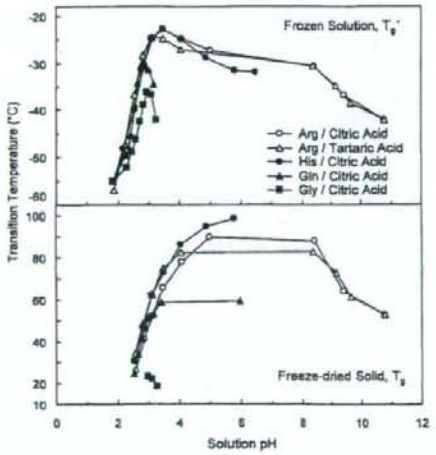

Fig. 6. Effect of Initial Solution pH (25 °C) on the Transition Temperatures of Frozen Solutions (T_g') and Freeze-Dried Solids (T_g) Containing an Amino Acid and an Organic Acid at a Fixed (0.1) Molar Concentration Ratio Intervals (200 mM Total, $n=3$)

Transition temperatures (T_g', T_g) of the excipient combinations obtained at a fixed (0.1) molar ratio interval were plotted against the pH of the initial solutions (25 °C, Fig. 6). Some mixtures (*e.g.*, L-arginine and citric acid, L-histidine and citric acid) yielded high T_g' frozen solutions and high T_g freeze-dried solids from weakly acidic initial solutions ($-35\,°C<T_g'$, $80\,°C<T_g$, pH 4—6), which are preferable in parenteral protein formulations. Small changes in the L-arginine and organic acid compositions (0.1 molar fraction) significantly shifted pH at the neutral region.

The mid- and near-infrared spectra of the freeze-dried L-arginine and citric acid combinations showed broad absorption bands that are typical of amorphous solids (Figs. 7, 8).[21] Co-lyophilization with citric acid reduced an amino group absorption band of L-arginine at 1550 cm^{-1} in the mid-IR spectra (KBr method), indicating altered environment of the functional group. Similar reduction of the amino group band has been reported in L-arginine–HCl salt crystal and L-argi-

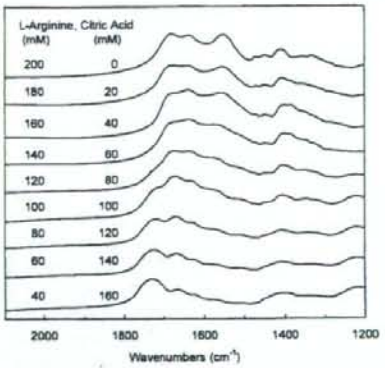

Fig. 7. Mid-Infrared Spectra of Freeze-Dried L-Arginine and Citric Acid Combinations Obtained by a KBr Tablet Method (128 Scans)

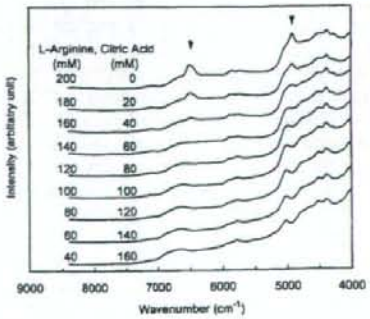

Fig. 8. Diffuse-Reflection Near-Infrared Spectra of Freeze-Dried L-Arginine and Citric Acid Combinations Obtained at the Bottom of the Glass Vials (128 Scans)

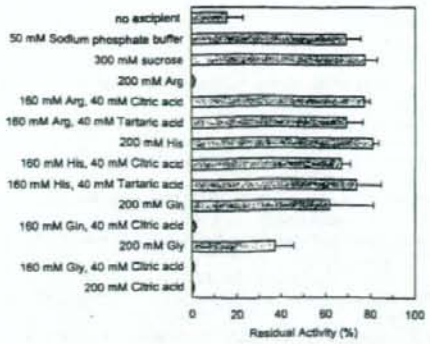

Fig. 9. Effect of Amino Acid and Organic Acid Combinations on the Activity of Freeze-Dried Lactate Dehydrogenase (50 μg/ml, Average±S.D., $n=3$)

nine freeze-dried with inorganic acids (*e.g.*, HCl, H_3PO_4).[13] A carboxyl group band at 1725 cm^{-1} appeared when the citric acid ratio was increased. Diffuse-reflection near-infrared spectra obtained non-destructively at the bottom of the glass vials also indicated the altered local environment of the functional groups. A large amino band of L-arginine (6505 cm^{-1}, N–H stretching 1st overtone) disappeared in the presence of lower molar concentration ratio of citric acid in the initial solution (140 mM L-arginine, 60 mM citric acid). Increasing the citric acid ratio also reduced the large absorption band at 4920 cm^{-1}, and concomitantly induced band at 5030 cm^{-1} in the co-lyophilized solids. Assignment of these bands remains to be elucidated. The results strongly suggested hydrogen-bonding and/or electrostatic interactions between L-arginine and citric acid in the lyophilized solids.

Effect of Excipients on Inactivation of Freeze-Dried LDH Freeze-drying of LDH in the absence of the stabilizing excipients resulted in significant reduction of the activity (approximately 15% of the initial solution) (Fig. 9). Higher enzyme activity was retained in freeze-drying at a higher phosphate buffer concentration (50 mM). Some amino acid and organic acid combinations that provide neutral to weakly acidic initial solution (pH 5—8) and amorphous dried solids also retained the enzyme activity. The enzyme lost most of the activity in freeze-drying from extreme pH solutions (*e.g.*, 200 mM L-arginine, pH 10.6). Addition of citric acid or L-tartaric acid slightly reduced the effect of L-histidine to retain the activity of LDH during freeze-drying. Crystallization of glycine in the single-solute frozen solution, and concomitant loss of the protecting effect, should explain the lower remaining enzyme activity.[1,2,22]

Discussion

The freeze-drying of aqueous solutions containing some basic or neutral amino acid (*e.g.*, L-arginine, L-histidine) and hydroxy di- or tricarboxylic acid (*e.g.*, citric acid, L-tartaric acid) combinations resulted in the glass-state amorphous solid cakes that protect proteins from dehydration stresses. Some of the solids showed glass transition temperatures comparable to those of disaccharides (*e.g.*, sucrose, trehalose).[4] The data and recent literature on the properties of related substances in different physical states (*e.g.*, complex crystals, ionic liquids) strongly suggested contribution of the multiple functional groups of the consisting molecules to form the interaction (*e.g.*, electrostatic, hydrogen-bonding) networks required for the glass-state amorphous solids.[23—25] Multiple amino, carboxyl, and hydroxyl groups in the solute molecules raise transition temperatures of the mixture frozen solutions (T_g') and the freeze-dried solids (T_g).[15] The ammonium carbohydrate ion pairs form multiple hydrogen-bondings in some non-polar solvents.[23,24] Differently protonated carboxyl and carboxylate groups also form an intermolecular hydrogen-bonding network.[25]

The amino acids and organic acids containing plural amino or carboxyl groups should have large chance to form the interactions with multiple counterpart molecules. The contribution of the multiple functional groups should explain the high transition temperatures (T_g', T_g) of the L-arginine and citric acid combination. L-Arginine also forms stable amorphous freeze-dried solids with multivalent inorganic acids (*e.g.*, H_3PO_4).[11,13] Frozen sodium citrate and tartrate buffer solutions exhibit the highest T_g' at certain sodium concentration ratios.[17] Supramolecular interactions (*e.g.*, peptide-like periodic interactions) reported in some complex crystals of amino acid and dicarboxylic acid (*e.g.*, L-arginine and adipic acid, X-ray analysis)[26] should support the possible multi-molecular interaction network in the less-ordered amorphous phase.

Hydroxyl groups in the citric acid, L-tartaric acid, and DL-malic acid should introduce additional hydrogen bonding to the amorphous phase. The number of hydroxyl groups in the component, and the accompanying change in the molecular interactions are major factors in determining the glass transition temperature of some ionic liquids composed of an amino acid and a 1-allylimidazolium cation.[27] The intense interactions and resulting reduction of the molecular mobility may prevent the crystallization of amino acids (*e.g.*, glycine, glutamine) at concentration ratios much lower than those of "inert" nonionic solutes (*e.g.*, sucrose) or inorganic salts (*e.g.*, NaCl).[17,30—32]

The high glass transition temperature amorphous solids formed by combinations of popular excipients would be a practical alternative to disaccharides in the design of freeze-dried protein formulations. The excipient combinations would satisfy the two major protein-stabilizing mechanisms postulated on saccharides, namely substitution of the surrounding water molecules by hydrogen-bonding and reduction of the chemical reaction by embedding in the glass-state solids.[6—8] Additional effects of some amino acids (*e.g.*, reduced aggregation in aqueous solution by L-arginine) preferable in protein formulations are also anticipated.[9] The limited crystallinity and low volatility of the amino acid and organic acid should reduce the risk of pH change and the resulting protein inactivation in the freeze-drying process reported in some buffer systems.[28]

Various proteins degrade during the freeze-drying process and subsequent storage through several chemical and physical mechanisms.[3,29] The low concentration LDH solution is often used as a model system for studying the effect of co-solutes in the freeze-thawing and freeze-drying processes because of its apparent tendency to lose its activity due to irreversible subunit dissociation and conformation change.[30] The ability of excipient combinations to retain the enzyme

activity in the freeze-drying process should indicate the stabilization of the quarterly structure against freeze-concentration and dehydration stress. Different molecular mobility, local pH, water content, and crystallinity of the excipients may affect the chemical degradation rate of the freeze-dried enzyme in the subsequent storage. The freeze-dried basic amino acid and organic acid combination solids should provide the embedded proteins with unique local environments that are significantly different from those of the nonionic excipients (*e.g.*, saccharides). The structural and chemical stability of proteins in these solids during the freeze-drying process and storage is an intriguing topic that needs further study through various model protein and stress systems.

References

1) Nail S. L., Jiang S., Chongprasert S., Knopp S. A., *Pharm. Biotechnol.*, **14**, 281—360 (2002).
2) Tang X., Pikal M. J., *Pharm. Res.*, **21**, 191—200 (2004).
3) Carpenter J. F., Arakawa T., Crowe J. H., *Dev. Biol. Stand.*, **74**, 225—238 (1992).
4) Franks F., *Dev. Biol. Stand.*, 74, 9—18 (1992).
5) Lee J. C., Timasheff S. N., *J. Biol. Chem.*, **256**, 7139—7201 (1981).
6) Chang B. S., Randall C., *Cryobiology*, **29**, 632—656 (1992).
7) Arakawa T., Timasheff S. N., *Arch. Biochem. Biophys.*, **224**, 169—177 (1983).
8) Sane S. U., Wong R., Hsu C. C., *J. Pharm. Sci.*, **93**, 1005—1018 (2004).
9) Tsumoto K., Umetsu M., Kumagai I., Ejima D., Philo J. S., Arakawa T., *Biotechnol. Prog.*, **20**, 1301—1308 (2004).
10) Osterberg T., Fatouros A., Mikaelsson M., *Pharm. Res.*, **14**, 892—898 (1997).
11) Mattern M., Winter G., Kohnert U., Lee G., *Pharm. Dev. Technol.*, **4**, 199—208 (1999).
12) Osterberg T., Wadsten T., *Eur. J. Pharm. Sci.*, **8**, 301—308 (1999).
13) Izutsu K., Fujinaki Y., Kuwabara A., Aoyagi N., *Int. J. Pharm.*, **301**, 161—169 (2005).
14) Li J., Chatterjee K., Medek A., Shalaev E., Zografi G., *J. Pharm. Sci.*, **93**, 697—712 (2004).
15) Kadoya S., Izutsu K., Yonemochi E., Terada K., Yomota C., Kawanishi T., *Chem. Pharm. Bull.*, **56**, 821—826 (2008).
16) Akers M. J., Milton N., Byrn S. R., Nail S. L., *Pharm. Res.*, **12**, 1457—1461 (1995).
17) Shalaev E. Y., Johnson-Elton T. D., Chang L., Pikal M. J., *Pharm. Res.*, **19**, 195—201 (2002).
18) Chongprasert S., Knopp S. A., Nail S. L., *J. Pharm. Sci.*, **90**, 1720—1728 (2001).
19) Lu Q., Zografi G., *J. Pharm. Sci.*, **86**, 1374—1378 (1997).
20) Shamblin S. L., Taylor L. S., Zografi G., *J. Pharm. Sci.*, **87**, 694—701 (1998).
21) Yonemochi E., Inoue Y., Buckton G., Moffat A., Oguchi T., Yamamoto K., *Pharm. Res.*, **16**, 835—840 (1999).
22) Anchordoquy T. J., Carpenter J. F., *Arch. Biochem. Biophys.*, **332**, 231—238 (1996).
23) Sada K., Tani T., Shinkai S., *Synlett*, **2006**, 2364—2374 (2006).
24) Yerger E. A., Barrow G. M., *J. Am. Chem. Soc.*, 77, 6206—6207 (1955).
25) Kobayashi N., Naito T., Inabe T., *Bull. Chem. Soc. Jpn.*, **76**, 1351—1362 (2003).
26) Roy S., Singh D. D., Vijayan M., *Acta Crystallogr. B*, **61**, 89—95 (2005).
27) Fukumoto K., Yoshizawa M., Ohno H., *J. Am. Chem. Soc.*, **127**, 2398—2399 (2005).
28) Li J., Guo Y., Zografi G., *Pharm. Res.*, **19**, 20—26 (2002).
29) Manning M. C., Patel K., Borchardt R. T., *Pharm. Res.*, **6**, 903—918 (1989).
30) Seguro K., Tamiya T., Tsuchiya T., Matsumoto J. J., *Cryobiology*, **27**, 70—79 (1990).

Feasibility of ^{19}F-NMR for Assessing the Molecular Mobility of Flufenamic Acid in Solid Dispersions

Yukio Aso,* Sumie Yoshioka, Tamaki Miyazaki, and Toru Kawanishi

National Institute of Health Sciences; 1–18–1 Kamiyoga, Setagaya, Tokyo 158–8501, Japan.
Received September 9, 2008; accepted October 22, 2008; published online October 23, 2008

The purpose of the present study was to clarify the feasibility of ^{19}F-NMR for assessing the molecular mobility of flufenamic acid (FLF) in solid dispersions. Amorphous solid dispersions of FLF containing poly(vinylpyrrolidone) (PVP) or hydroxypropylmethylcellulose (HPMC) were prepared by melting and rapid cooling. Spin–lattice relaxation times (T_1 and $T_{1\rho}$) of FLF fluorine atoms in the solid dispersions were determined at various temperatures (−20 to 150 °C). Correlation time (τ_c), which is a measure of rotational molecular mobility, was calculated from the observed T_1 or $T_{1\rho}$ value and that of the T_1 or $T_{1\rho}$ minimum, assuming that the relaxation mechanism of spin–lattice relaxation of FLF fluorine atoms does not change with temperature. The τ_c value for solid dispersions containing 20% PVP was 2—3 times longer than that for solid dispersions containing 20% HPMC at 50 °C, indicating that the molecular mobility of FLF in solid dispersions containing 20% PVP was lower than that in solid dispersions containing 20% HPMC. The amount of amorphous FLF remaining in the solid dispersions stored at 60 °C was successfully estimated by analyzing the solid echo signals of FLF fluorine atoms, and it was possible to follow the overall crystallization of amorphous FLF in the solid dispersions. The solid dispersion containing 20% PVP was more stable than that containing 20% HPMC. The difference in stability between solid dispersions containing PVP and HPMC is considered due to the difference in molecular mobility as determined by τ_c. The molecular mobility determined by ^{19}F-NMR seems to be a useful measure for assessing the stability of drugs containing fluorine atoms in amorphous solid dispersions.

Key words ^{19}F-NMR; molecular mobility; stability; crystallization; solid dispersion

Amorphous solid dispersions are used for improving the dissolution rate and solubility of poorly soluble drugs. However, drugs in amorphous form are generally less stable than crystalline drugs because of their higher energy state and higher molecular mobility. It is well known that polymeric excipients can reduce the crystallization rate of many amorphous drugs.[1—12] This stabilization by poly(vinylpyrrolidone) (PVP) is partly attributable to its ability to decrease molecular mobility, as indicated by increases in the glass transition temperature (T_g).[9] Therefore, it is of great interest to estimate the molecular mobility of drugs in solid dispersions. Although ^{13}C-NMR relaxation measurements are useful for assessing the molecular mobility of drugs in solid dispersions,[13] the low sensitivity of ^{13}C because of its low natural abundance is a drawback of ^{13}C-NMR. In contrast to ^{13}C, ^{19}F has very favorable sensitivity in NMR experiments, since it is present in 100% natural abundance, is second only to the proton in its resonance frequency (except ^{3}H) and has a spin quantum number of 1/2. The receptivity for ^{19}F is 83% of that for ^{1}H and 4700 times of that for ^{13}C.[14] Many drugs containing fluorine atoms are listed in The Japanese Pharmacopoeia. In contrast, almost all pharmaceutical excipients do not contain fluorine atoms. ^{19}F-NMR may therefore have an advantage over ^{13}C-NMR or ^{1}H-NMR for selectivity and sensitivity when assessing the molecular mobility of drugs containing fluorine atoms in pharmaceutical dosage forms such as solid dispersions.

The orientations and molecular mobility of flufenamic acid (FLF)[15] and ^{19}F-labeled α-tocopherol[16] in a lipid bilayer were studied using ^{19}F-NMR. Structures and molecular mobility of ^{19}F-labeled peptides and proteins in biological membranes were also investigated.[17—20] To the authors' knowledge, application of ^{19}F-NMR to studies of drug molecular mobility in solid dispersions has not been reported. This paper describes the feasibility of ^{19}F-NMR for assessing the molecular mobility of FLF in PVP or hydroxypropylmethylcellulose (HPMC) solid dispersions, and discusses the effect of polymer excipients on the crystallization tendency of FLF in solid dispersions in terms of differences in molecular mobility.

Experimental

Materials FLF (Fig. 1) was purchased from Wako Pure Chemical Industry (Osaka), and PVP and HPMC were from Sigma (St. Louis, MO, U.S.A.). FLF solid dispersions with PVP or HPMC were prepared by melting and cooling of mixtures of FLF with PVP or HPMC. The solid dispersions obtained were confirmed to be amorphous from microscopic observation under polarized light.

Nuclear Magnetic Relaxation Measurements ^{19}F-NMR measurements were carried out using a model JNM-MU25 pulsed NMR spectrometer (JEOL DATUM, Tokyo) operating at a resonance frequency of 25 MHz. Time profiles of spin–spin relaxation of the ^{19}F atoms of FLF were measured using the "solid echo" pulse sequence to overcome the dead time of the instrument. Spin–lattice relaxation time in the laboratory frame (T_1) was measured using the inversion recovery pulse sequence. Spin–lattice relaxation time in the rotating flame ($T_{1\rho}$) was measured at spin locking intensity of 10 G.

DSC Measurements T_g of FLF-PVP and FLF-HPMC solid dispersions was measured by DSC using a model 2920 differential scanning calorimeter and a refrigerator cooling system (TA Instruments, Newcastle, DE, U.S.A.). Approximately 5 mg of each solid dispersions was put into an aluminum sample pan and then sealed hermetically. T_g was measured at a heating rate of 20 °C/min. Temperature calibration of the instrument was carried out using indium.

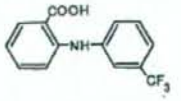

Fig. 1. Structure of FLF

* To whom correspondence should be addressed. e-mail: aso@nihs.go.jp

Results and Discussion

Molecular Mobility of FLF as Measured by ^{19}F-NMR Spin–Lattice Relaxation Time T_1 and $T_{1\rho}$ of fluorine atoms of FLF in PVP and HPMC solid dispersions were measured using a pulsed NMR spectrometer in the temperature range from −20 to 150 °C. T_1 is sensitive to the molecular motion on the time scale of the resonance frequency (MHz order). On the other hand, $T_{1\rho}$ is sensitive to the molecular motion with a frequency equivalent to the intensity of spin locking field (typically mid kHz order).[21] The temperature dependence of T_1 and $T_{1\rho}$ exhibits minimum at a specific temperature at which the molecules of interest have molecular motion with MHz time scale or mid kHz time scale predominantly. The resonance frequency of 25 MHz, lower than that of a conventional high resolution NMR spectrometer, was used to observe T_1 minimum in the temperature rage studied. Figure 2 shows the temperature dependence of T_1 and $T_{1\rho}$ of FLF fluorine atoms in PVP and HPMC solid dispersions. For FLF–PVP solid dispersions (7 : 3), the minimum of T_1 or $T_{1\rho}$ was observed at about 90 °C and 60 °C, respectively (Fig. 2A). When the PVP content decreased to 20% (w/w), T_1 and $T_{1\rho}$ of FLF at temperatures above 70 °C could not be determined due to rapid crystallization. Similar temperature dependence of T_1 or $T_{1\rho}$ was observed for the FLF–HPMC solid dispersions (Fig. 2B). The temperature difference between T_1 and $T_{1\rho}$ minimum is considered to be due to the difference in the time scale of molecular motion reflected on T_1 (MHz order) and $T_{1\rho}$ (mid kHz order). Since the molecular motion on MHz time scale becomes predominant at higher temperature than molecular motion on mid kHz time scale, T_1 minimum is observed at higher temperature than $T_{1\rho}$ minimum.

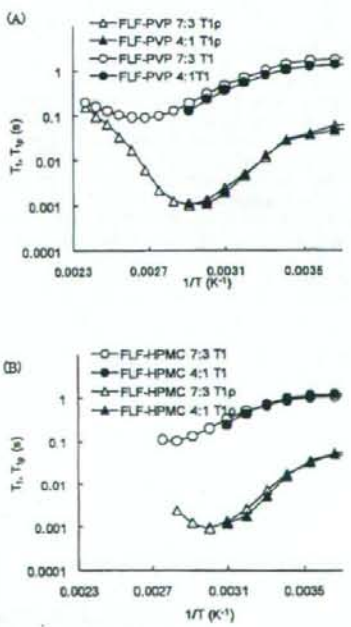

Fig. 2. Temperature Dependence of T_1 and $T_{1\rho}$ of FLF Fluorine Atoms in PVP (A) and HPMC (B) Solid Dispersions

We made following assumptions in order to estimate the molecular mobility of FLF from T_1 and $T_{1\rho}$ of FLF fluorine atoms: first, we assumed that FLF fluorine atoms in the solid dispersions relaxes mainly *via* dipolar interaction, and that the contribution of the spin–rotation interaction mechanism[21] is negligible. While relaxation *via* the spin–rotation interaction mechanism has been reported for liquid sample,[22—24] complete domination of dipolar interactions has been reported for fluorine atoms for polycrystalline van der Waals molecular solid.[25] We also made an assumption that the contribution of the cross-relaxation between fluorine and proton atoms can be considered small. It is known that relaxation is not intrinsically single-exponential when cross-relaxation between fluorine and proton atoms takes place.[14] However, we assumed small contribution of the cross-relaxation, because the relaxation of FLF fluorine atoms in the solid dispersions was exponential within experimental uncertainty. In studies of molecular motions, a large number of models describing molecular motions have been proposed for calculation of the spectrum density function.[26] We used a simple model that the molecular motion reflected on T_1 or $T_{1\rho}$ is represented by single correlation time for the purpose of comparing the mobility of FLF in the PVP and HPMC solid dispersions. According to the above assumptions, T_1 and $T_{1\rho}$ are described by Eqs. 1 and 2.[21]

$$\frac{1}{T_1} = \frac{6}{20}\frac{\gamma^4\hbar^2}{r^6}\left\{\frac{\tau_c}{1+\omega_0^2\tau_c^2} + \frac{4\tau_c}{1+4\omega_0^2\tau_c^2}\right\} \quad (1)$$

$$\frac{1}{T_{1\rho}} = \frac{3}{20}\frac{\gamma^4\hbar^2}{r^6}\left\{\frac{3\tau_c}{1+4\omega_1^2\tau_c^2} + \frac{5\tau_c}{1+\omega_0^2\tau_c^2} + \frac{2\tau_c}{1+4\omega_0^2\tau_c^2}\right\} \quad (2)$$

where τ_c is the correlation time that characterizes molecular reorientations, and ω_0 and ω_1 are the resonance frequencies of fluorine atoms in the static magnetic field and spin locking field, respectively. γ, r and $\hbar$ are the gyromagnetic ratio of fluorine, the distance of neighboring fluorine atoms, and the Plank constant divided by 2π, respectively. Equations 1 and 2 infer that T_1 and $T_{1\rho}$ become minimal when $\omega_0\tau_c$ is approximately 0.62[27] and $\omega_1\tau_c$ is approximately 0.52,[21] respectively. When the minimum of T_1 or $T_{1\rho}$ is observed, we can calculate the unknown value, r, in Eqs. 1 and 2. If r is known, the τ_c value can be calculated from the observed T_1 or $T_{1\rho}$ value, assuming that r does not change with temperature.

The values of r calculated from the T_1 and $T_{1\rho}$ minimum observed for the FLF–PVP solid dispersion (7 : 3) were 2.3 and 2.4 Å, respectively, and similar r values were obtained for the FLF–HPMC solid dispersion (7 : 3). These values are comparable to the reported value (2.174 Å) for 3-(trifluoromethyl)phenanthrene,[25] indicating that dipole interaction between neighboring fluorine atoms can be considered the predominant relaxation mechanism of FLF fluorine atoms in the solid dispersions. The difference between the r values obtained in this work and the reported value suggests that the possibility of the spin–rotation interaction mechanism and/or dipole interaction between fluorine and proton atoms cannot be excluded as a relaxation mechanism of FLF fluorine atoms.

Figure 3 shows the temperature dependence of τ_c calculated from T_1 and $T_{1\rho}$ for FLF fluorine atoms in the solid dis-

persions. The τ_c of FLF fluorine atoms in PVP solid dispersions calculated from $T_{1\rho}$ was 8.2 μs at 50 °C, which was about 3 times larger than that in HPMC solid dispersions (2.6 μs), indicating that the molecular mobility of FLF was lowered more strongly by PVP than by HPMC.

The τ_c values calculated using T_1 values differ from those calculated from $T_{1\rho}$ values. The slope of temperature dependence of τ_c changed around T_g. These findings suggest that the assumption that the molecular motion reflected on T_1 and $T_{1\rho}$ is represented by a single τ_c may be too simple to describe the molecular motion of FLF in the solid dispersions at temperatures studied, and that two or more molecular motions, such as rotation of trifluoromethyl group and motions with larger scales than rotation of trifluoromethyl group, may be reflected on T_1 and $T_{1\rho}$. Further studies including ^{1}H-NMR relaxation measurement and dielectric relaxation measurements will be needed to identify the detailed molecular motion of FLF in the solid dispersions.

Correlation between Crystallization Tendency and Molecular Mobility of FLF in Solid Dispersions Crystallization proceeds *via* formation of crystal nuclei and crystal growth. As a measure of the crystallization tendency of amorphous FLF in solid dispersions, the overall crystallization rate of amorphous FLF in the solid dispersions was estimated from the time profiles amorphous FLF remaining in the solid dispersions instead of measuring the nucleation rate and growth rate. Amorphous FLF remaining in the solid dispersions was estimated by analyzing solid echo signals of FLF fluorine atoms. Figure 4 shows the solid echo signal of fluorine atoms of FLF in solid dispersions containing 20% (w/w) PVP and that of fluorine atoms of crystalline FLF. The signal for the solid dispersions was describable by the Lorentzian relaxation equation (Eq. 3), and its relaxation time (T_{2L}) was approximately 140 μs. Crystalline FLF exhibited Gaussian relaxation signals (Eq. 4), and its relaxation time (T_{2G}) was approximately 30 μs. These results indicate that amorphous FLF in solid dispersions is considered to exhibit Lorentzian relaxation signals.

$$I=I_0\exp(-t/T_{2L}) \tag{3}$$

$$I=I_0\exp\{-t^2/(2T_{2G}^2)\} \tag{4}$$

where I_0 and I represent the signal intensities at time 0 and t, respectively. Figure 5 shows solid echo signals for the fluorine atoms of FLF in the solid dispersions stored at 60 °C. Samples stored at 60 °C exhibited biphasic decay signals, and signals were describable by summation of the Gaussian (solid line) and Lorentzian (dashed line) equations (Eq. 5).

$$I=I_0\{P_L\exp(-t/T_{2L})+P_G\exp(-t^2/2T_{2G}^2)\} \tag{5}$$

where P_L and P_G are the ratio of fluorine atoms exhibiting Lorentzian and Gaussian relaxation process, respectively, and $P_L+P_G=1$. Assuming that the T_{2L} and T_{2G} values are 140 and 30 μs, respectively, P_L values of FLF in the solid dispersions were estimated by curve fitting. P_L values of the solid dispersions decreased with increasing storage time, indicating that crystallization of amorphous FLF in solid dispersions takes place during storage at 60 °C. To certify the reliability of the P_L values obtained by ^{19}F-NMR measurements, change in the heat capacity at T_g ($\Delta C_p(T_g)$) was determined for the solid dispersions stored at 60 °C for various periods as a measure of amorphous FLF remaining, and was compared with the value of P_L. As shown in Fig. 6, the P_L value was proportional to the $\Delta C_p(T_g)$ value, and was considered to be a useful measure of amorphous FLF remaining in the solid dispersions.

Figure 7 shows the time profiles of the P_L values for FLF solid dispersions containing 20% (w/w) PVP or HPMC at 60 °C. The decrease in the ratio of Lorentzian fluorine atoms was faster for HPMC solid dispersions than for PVP solid dispersions, indicating that the overall crystallization rate of FLF in HPMC solid dispersions is larger than that in PVP solid dispersions. The overall crystallization rate depends on both molecular mobility (the rate of diffusion across the interface between crystalline and amorphous phase) and ther-

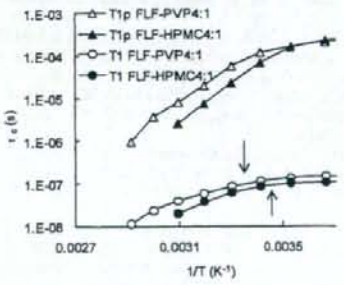

Fig. 3. Temperature Dependence of τ_c of FLF Fluorine Atoms in PVP and HPMC Solid Dispersions

Arrows in the figure represent T_g.

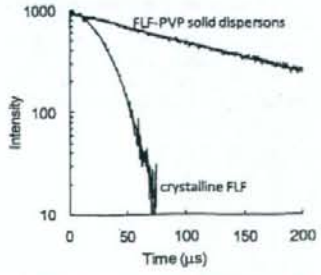

Fig. 4. Typical Solid Echo Signal of Fluorine Atoms of FLF in the Freshly Prepared Solid Dispersion Containing 20% (w/w) PVP and That of Fluorine Atoms of Crystalline FLF

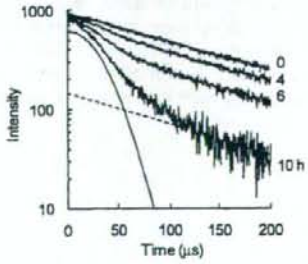

Fig. 5. Typical Solid Echo Signals of Fluorine Atoms of FLF in the Solid Dispersions Containing 20% (w/w) PVP Stored at 60 °C

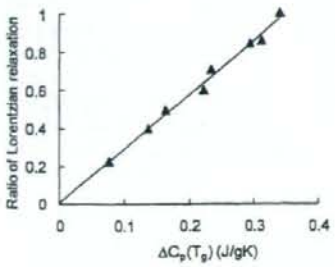

Fig. 6. The Ratio of FLF Fluorine Atoms Exhibiting Lorentzian Relaxation as a Function of Changes in the Heat Capacity at T_g

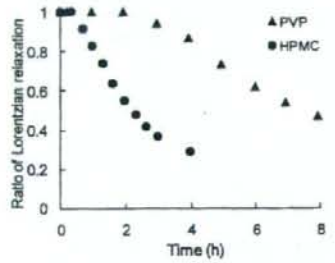

Fig. 7. Time Profiles of the Ratio of FLF Fluorine Atoms Exhibiting Lorentzian Relaxation in PVP and HPMC Solid Dispersions Stored at 60 °C

modynamic factors, such as free energy difference between crystalline and amorphous form.[2,3,10] Differences in the overall crystallization rate of amorphous FLF are consistent with those in the molecular mobility (Fig. 3), suggesting that the molecular mobility as determined by the ^{19}F-NMR spin–lattice relaxation times may be one of the factors determining crystallization rate, and useful as a measure of the physical stability of FLF in solid dispersions. The T_g values of the solid dispersions containing 20% PVP and 20% HPMC were 23 °C and 15 °C, respectively, indicating that molecular mobility reflected on T_g is higher for the solid dispersion containing HPMC than for that containing PVP. The T_g data seem to support the speculation obtained from NMR data. However, the scale of molecular mobility reflected on T_g is considered to be larger than that reflected on τ_c. Further studies should be conducted to elucidate the quantitative correlation between the physical stability of amorphous FLF and the molecular mobility determined by ^{19}F-NMR.

In conclusion, ^{19}F-NMR is useful for elucidating the molecular mobility of drugs containing fluorine atoms in amorphous solid dispersions. τ_c values of FLF fluorine atoms were calculated from the ^{19}F-NMR spin–lattice relaxation data. The τ_c value for solid dispersions containing 20% PVP was 2—3 times longer than that for solid dispersions containing 20% HPMC at 50 °C. Molecular mobility of FLF in the solid dispersions containing 20% PVP was lower than in those containing 20% HPMC, and this was consistent with the fact that the overall crystallization rate of amorphous FLF in the solid dispersion containing PVP was smaller than in that containing HPMC. The molecular mobility determined by ^{19}F-NMR seems to be useful as a measure of the physical stability of an amorphous drug in solid dispersions.

Acknowledgements Part of this work was supported by a Grant-in-aid for Research on Publicly Essential Drugs and Medical Devices from The Japan Health Sciences Foundation.

References

1) Yoshioka M., Hancock B. C., Zografi G., *J. Pharm. Sci.*, **84**, 983—986 (1995).
2) Matsumoto T., Zografi G., *Pharm. Res.*, **16**, 1722—1728 (1999).
3) Crowley K. J., Zografi G., *Pharm. Res.*, **20**, 1417—1422 (2003).
4) Shamblin S. L., Huang E. Y., Zografi G., *J. Therm. Anal.*, **47**, 1567—1579 (1996).
5) Shamblin S. L., Zografi G., *Pharm. Res.*, **16**, 1119—1124 (1999).
6) Zeng X. M., Martin G. P., Marriott C., *Int. J. Pharm.*, **218**, 63—73 (2001).
7) Miyazaki T., Yoshioka S., Aso Y., Kojima S., *J. Pharm. Sci.*, **93**, 2710—2717 (2004).
8) Khougaz K., Clas S., *J. Pharm. Sci.*, **89**, 1325—1334 (2000).
9) Berggren J., Alderborn G., *Eur. J. Pharm. Sci.*, **21**, 209—215 (2004).
10) Aso Y., Yoshioka S., Kojima S., *J. Pharm. Sci.*, **93**, 384—391 (2004).
11) Miyazaki T., Yoshioka S., Aso Y., *Chem. Pharm. Bull.*, **54**, 1207—1210 (2006).
12) Konno H., Taylor L. S., *J. Pharm. Sci.*, **95**, 2692—2705 (2006).
13) Aso Y., Yoshioka S., *J. Pharm. Sci.*, **95**, 318—325 (2006).
14) Harris R. K., Monti G. A., Holstein P., "Solid State NMR of Polymers," Chap. 6, ed. by Ando I., Asakura T., Elsevier, Amsterdam, 1998, pp. 351—414.
15) Grage S. L., Ulrich A. S., *J. Magn. Reson.*, **146**, 81—88 (2000).
16) Urano S., Matsuo M., Sakanaka T., Uemura I., Koyama M., Kumadaki I., Fukuzawa K., *Arch. Biochem. Biophys.*, **303**, 10—14 (1993).
17) Afonin S., Glaser R. W., Berditchevskaia M., Wadhwani P., Gührs K. H., Möllmann U., Perner A., Ulrich A. S., *ChemBioChem*, **4**, 1151—1163 (2003).
18) Salgado J., Grage S. L., Kondejewski L. H., Hodges R. S., McElhaney R. N., Ulrich A. S., *J. Biomol. NMR*, **21**, 191—208 (2001).
19) Williams S. P., Haggie P. M., Brindle K. M., *Biophys. J.*, **72**, 490—498 (1997).
20) Quint P., Ayala I., Busby S. A., Chalmers M. J., Griffin P. R., Rocca J., Nick H. S., Silverman D. N., *Biochemistry*, **45**, 8209—8215 (2006).
21) Farrar T. C., Becker E. D., "Pulse and Fourier Transform NMR," Academic Press, New York and Lodon, 1971.
22) Namgoong H., Lee J. W., *Bull. Korean Chem. Soc.*, **14**, 91—95 (1993).
23) Huang S.-G., Rogers M. T., *J. Chem. Phys.*, **68**, 5601—5606 (1978).
24) Gutowsky H. S., Lawrenceson I. J., Shimomura K., *Phys. Rev. Lett.*, **6**, 349—351 (1961).
25) Beckmann P. A., Rosenberg J., Nordstrom K., Mallory C. W., Mallory F. B., *J. Phys. Chem. A*, **110**, 3947—3953 (2006).
26) Horii F., "Solid State NMR of Polymers," Chap. 3, ed. by Ando I., Asakura T., Elsevier, Amsterdam, 1998, pp. 51—82.
27) Ruan R. R., Chen P. L., "Water in Foods and Biological Materials," Chap. 7, Technomic Publishing Co., Lancaster Basel, 1998, pp. 253—278.